AFRL-RY-HS-TR-2009-0038

ELECTROMAGNETIC COMPONENT RESEARCH

Richard T. Webster, J. Robert Reid, Everett E. Crisman, and A.F.M. Anwar
Sensors Directorate
Electromagnetics Technology Division
80 Scott Drive
Hanscom AFB MA 01731-2909

Final Technical Report

December 2009

DISTRIBUTION A: APPROVED FOR PUBLIC RELEASE, DISTRIBUTION UNLIMITED

AIR FORCE RESEARCH LABORATORY
Sensors Directorate
Electromagnetics Technology Division
80 Scott Drive
Hanscom AFB MA 01731-2909

NOTICE AND SIGNATURE PAGE

Using Government drawings, specifications, or other data included in this document for any purpose other than Government procurement does not in any way obligate the U.S. Government. The fact that the Government formulated or supplied the drawings, specifications, or other data does not license the holder or any other person or corporation; or convey any rights or permission to manufacture, use, or sell any patented invention that may relate to them.

Qualified requestors may obtain copies of this report from the Defense Technical Information Center (DTIC) (http://www.dtic.mil).

AFRL-RY-HS-TR-2009-0038 HAS BEEN REVIEWED AND IS APPROVED FOR PUBLICATION IN ACCORDANCE WITH ASSIGNED DISTRIBUTION STATEMENT.

Richard T. Webster

RICHARD T. WEBSTER
Work Unit Manager
Antenna Technology Branch
Electromagnetics Technology Division

David D. Curtis

DAVID D. CURTIS
Branch Chief
Antenna Technology Branch
Electromagnetics Technology Division

M. N. Alexander

MICHAEL N. ALEXANDER
Technical Advisor
Electromagnetic Technology Division

This report is published in the interest of scientific and technical information exchange, and its publication does not constitute the Government's approval or disapproval of its ideas or findings.

REPORT DOCUMENTATION PAGE

Form Approved
OMB No. 0704-0188

Public reporting burden for this collection of information is estimated to average 1 hour per response, including the time for reviewing instructions, searching data sources, gathering and maintaining the data needed, and completing and reviewing the collection of information. Send comments regarding this burden estimate or any other aspect of this collection of information, including suggestions for reducing this burden to Washington Headquarters Service, Directorate for Information Operations and Reports, 1215 Jefferson Davis Highway, Suite 1204, Arlington, VA 22202-4302, and to the Office of Management and Budget, Paperwork Reduction Project (0704-0188) Washington, DC 20503.
PLEASE DO NOT RETURN YOUR FORM TO THE ABOVE ADDRESS.

1. REPORT DATE *(DD-MM-YYYY)*	2. REPORT TYPE	3. DATES COVERED *(From - To)*
07-12-2009	Final Report	October 2001-September 2009

4. TITLE AND SUBTITLE
Electromagnetic Component Research

5a. CONTRACT NUMBER

5b. GRANT NUMBER

5c. PROGRAM ELEMENT NUMBER
61102F

6. AUTHOR(S)
Richard T. Webster, J. Robert Reid, Everett E. Crisman, and A. F. M. Anwar

5d. PROJECT NUMBER
2305

5e. TASK NUMBER
HA

5f. WORK UNIT NUMBER
01

7. PERFORMING ORGANIZATION NAME(S) AND ADDRESS(ES)
Sensors Directorate
Air Force Research Laboratory
80 Scott Dr
Hanscom AFB MA 01731

8. PERFORMING ORGANIZATION REPORT NUMBER
AFRL-RY-HS-TR-2009-0038

9. SPONSORING/MONITORING AGENCY NAME(S) AND ADDRESS(ES)
Sensors Directorate
Air Force Research Laboratory
80 Scott Dr
Hanscom AFB MA 01731

10. SPONSOR/MONITOR'S ACRONYM(S)
AFRL/RYHA

11. SPONSORING/MONITORING AGENCY REPORT NUMBER
AFRL-RY-HS-TR-2009-0038

12. DISTRIBUTION AVAILABILITY STATEMENT
DISTRIBUTION A. Approved for public release; distribution unlimited.

13. SUPPLEMENTARY NOTES

14. ABSTRACT
This report documents basic research in electromagnetic components performed by members of the Antenna Technology Branch of the Air Force Research Laboratory in collaboration with on-site contractors. The work includes modeling and measurement of III-V compound semiconductor devices for microwave and millimeter-wave transmit and receive applications, investigations of the factors that limit lifetime of radio frequency micro-electro-mechanical switches, creation of new micro-electro-mechanical and micromachined electromagnetic components, and investigation of the potential of emerging material systems for application to components. The research was supported by the Air Force Office of Scientific Research under Laboratory Tasks 92SN04COR and 07RY06COR.

15. SUBJECT TERMS
electromagnetic components, electronic filters, compound semiconductor, monolithic microwave integrated circuit, micro-electro-mechanical systems, millimeter-wave components, nanotechnology, micro-robotics

16. SECURITY CLASSIFICATION OF:			17. LIMITATION OF ABSTRACT	18. NUMBER OF PAGES	19a. NAME OF RESPONSIBLE PERSON
a. REPORT	b. ABSTRACT	c. THIS PAGE	sar	38	Richard T. Webster
U	U	U			19b. TELEPONE NUMBER *(Include area code)*

CONTENTS

FIGURES

Figure Page

PREFACE

This final report documents in-house research performed by members of the Air Force Research Laboratory, Sensors Directorate, Electromagnetics Technology Division, Antenna Technology Branch during the period 1 October 2001 to 30 September 2009. The authors of this report wrote most of the words contained herein, but the report represents the contributions of many more people. The scientific and technical team included the following Air Force Civilian employees, Air Force military members, and on-site contractors, collaborators, and students.

Air Force civilian employees: Richard T. Webster, Dr. J. Robert Reid, Dr. John S. Derov, Dr. Alvin J. Drehman, Dr. Vladimir Vasilyev, Dr. Paul H. Carr, George A. Roberts, and John M. Moulton.

Air Force military members (rank at the time of their work here): Capt. Benjamin Crossley, Capt. Lavern Starman (PhD), Capt. Eric Marsh, Capt. Luke R. P. Porisch, 1Lt. James Sattler, 1Lt Katie L. Schaetzle.

On-site contractors: Prof. A. F. M. Anwar, Prof. Everett Crisman, Prof Luciano Boglione

AFRL/RYD Collaborators: Dr. Ronald A. Coutu, Dr Jack Ebel, Dr. Richard Strawser, Rebecca Cortez,

University Collaborators: Prof. Paul E Kladitis (Air Force Institute of Technology), Prof. Otto J. Gregory (University of Rhode Island), Prof. William Euler (University of Rhode Island)

Students: Gregory Barchard (Northeastern University), Elias Faraclas (University of Connecticut), Zack Hastings (Northeastern University), Syed S. Islam (University of Connecticut), M. Emre Karagozler (Carnegie Mellon University), Shang Li Wu (University of Connecticut)

The research team acknowledges the support of Antenna Technology Branch Chiefs Livio D. Poles and David D. Curtis, Branch Technical Advisors David D. Curtis and Dr. Boris Tomasic, Electromagnetics Technology Division Chief Emil R. Martinsek, Division Technical Advisor Dr. Michael Alexander, and AFRL Senior Scientists for Antennas, Dr Robert Mailloux and Dr. Hans Steyskal. We also thank Joanne LeClerke and Ashleyanne Van Detjen for excellent administrative support.

We gratefully acknowledge the support of the Air Force Office of Scientific Research through Laboratory Tasks 92SN04COR and 07SN06COR, and we appreciate the guidance provided by AFOSR Program Managers Dr. Gerald Witt and Dr. Kitt Reinhardt.

Finally, we are grateful for the leadership and counsel of our late Division Chief, Dr. Richard Payne. His dedication to maintaining the basic research mission of the Electromagnetics Technology Division inspires us toward excellence.

1.0 SUMMARY

The broad objective of the Electromagnetic Component Research task was to improve our fundamental understanding of phenomena that enable or limit the future development of electromagnetic components for antenna applications. Overviews of the research accomplishments are presented in this report with additional detail provided in publications and patents. A list of publications, patents and presentations is included in the Appendix.

Over the eight year period of performance, we explored many different technologies. Our research in semiconductor devices included physics-based modeling and measurement of III-V devices made from GaAs, InP, GaN and various III-V alloys. The work was driven by the emergence of new material layer structures that enable high performance devices for microwave and millimeter-wave applications. Generally, our work included experimental measurement of devices to validate the models. In the area of Radio Frequency (RF) Micro-Electro-Mechanical Systems (MEMS), our research included both the creation of new MEMS components and the investigation of contact physics with the goal of understanding the failure mechanisms that plagued the early implementations of MEMS. We adapted emerging three-dimensional fabrications methods to create innovative microwave and millimeter-wave components such as couplers, filters, and diplexers. The resulting 3D circuits promise highly integrated, low-cost, high-performance alternatives to waveguide and microstrip components. Among the emerging material systems we investigated are multi-ferroic polymers for tunable RF components, GaN nanowires for sensors and transistors, and AlN pyroelectrics for millimeter-wave sensors. We investigated novel sensor components including fiber-optic based strain gages and thermal sensors for millimeter-wave imaging. We initiated research on micro-robots based on spherical shells of silicon and silicon dioxide. As they mature, the micro-sensors could detect a variety of phenomena including acoustic, electromagnetic activity, motion, and biological or chemical agents.

Several research areas have been transitioned to exploratory development, in particular, the MEMS and 3D circuit work. Two areas will be continued under new research tasks. The *Ensemble Based Matter* task will explore the creation and physics of dynamic matter formed from an ensemble of coordinated of sub-cubic millimeter robots. *Antenna-Coupled Millimeter-Wave Detectors using Pyroelectric Thin Films* will research a sensor consisting of an antenna, resistive load, pyroelectric capacitor, and interconnects supported by a micromachined silicon dioxide membrane on a silicon substrate.

2.0 INTRODUCTION

This report documents the Electromagnetic Component Research work unit over the period 01 October 2001 to 30 September 2009. The broad objective of the research was to improve our fundamental understanding of phenomena that enable or limit the future development of electromagnetic components for antenna applications. A number of scientific and technical areas were investigated during the course of this effort, and the sections are organized around these areas. Section 3 will discuss our research in physics based modeling of semiconductor devices. Section 4 covers microelectromechanical and micromachined devices. Section 5 reports on nanowires, multiferroics, and pyroelectrics. Novel sensor components are the subject of Section 6. Section 7 presents conclusions and recommendations. The effort has been documented in a number of journal articles, patents, and technical reports which are listed in the Appendix. These publications are available through the Defense Technical Information Center and in on-line repositories.

3.0 SEMICONDUCTOR DEVICE RESEARCH

Our research in semiconductor devices included physics-based modeling and measurement of III-V devices made from GaAs, InP, GaN and various III-V alloys. The work was driven by the emergence of new material layer structures that enable high performance devices for microwave and millimeter-wave applications. Generally, our work included experimental measurement of devices to validate the models.

Subsections 3.1 and 3.2 discuss High Electron Mobility Transistors (HEMTs) with InGaAs channel layers. These transistor structures use a high mobility indium alloy in the channel region and can achieve low noise figure with high gain in the millimeter-wave range, making them suitable for receive amplifiers in high performance electronic systems. However, along with the high mobility, the indium-based channel layer has a narrow bandgap, leading to the onset of impact ionization at relatively low voltages. Impact ionization is a noisy process and can limit the low-noise performance of the device. Modeling of the impact ionization provides insight into process and guides design of high performance HEMTs.

In subsection 3.3, we report on our research in AlGaN/GaN HEMTs. GaN is a wide bandgap semiconductor and devices based on GaN can sustain high bias voltages and operate at higher temperatures compared to GaAs and InP based devices. These features make GaN HEMTs strong candidates for compact high power transistors in the microwave and millimeter-wave ranges.

3.1 Determination of Impact Ionization Gate Current InAlAs/InGaAs/InAlAs HEMTs

We devised a method to model the impact ionization gate current in InAlAs/InGaAs/InAlAs HEMTs. In the high electric field region of a HEMT, some electrons gain enough energy to produce holes and secondary electrons through impact ionization. Although the holes are confined to the channel by potential barriers of the HEMT quantum well, some fraction will tunnel through the barrier or have sufficient energy overcome the barrier and reach the gate. This hole current is proportional to the drain current, the impact ionization coefficient, the length of the high field region, and the probability of hole transmission through the gate potential barrier. We compute the ionization coefficient as a function of electric field using a Monte Carlo technique, calculating the fraction of electrons that participate in impact ionization as a function of electric field. The gate potential barrier is computed by solving the Schrödinger and Poisson's equations self-consistently to find the band bending and the two dimensional electron gas concentration in the channel as a function of the electric field at the heterointerface. The conduction band and valence band profiles can then be computed as a function of gate voltage. Next we use the Wentzel-Kramers-Broullion approximation to compute the hole transmission probability through the computed barrier. The ratio of the calculated channel hole current to the drain current follows the well known exponential dependence of the ionization constant when plotted as a function of reciprocal electric field. Fig. 1 shows the gate current due to impact ionization calculated from the current voltage characteristic shown in the inset and plotted as a function of source-drain bias (solid line). Experimental data points obtained using the extraction technique in [1] are shown for comparison. Theoretical calculations agree with the experimental measurements of the gate current in InP HEMTs. Further details of this technique will be submitted for publication as a journal article.

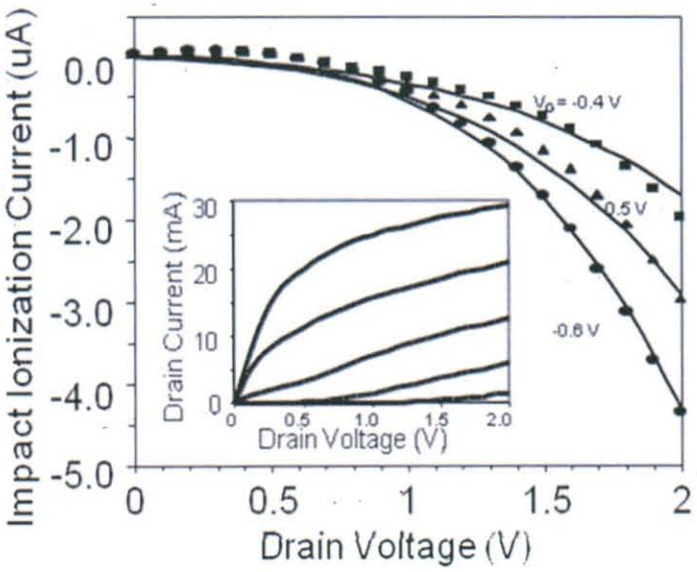

Figure 1: Gate Current due to Impact Ionization

3.2 AlGaAsSb/InGaAs/AlGaAsSb Metamorphic HEMTs

The impact ionization coefficient of AlGaAsSb/InGaAs/AlGaAsSb Metamorphic HEMTs (MHEMT) was experimentally determined by extracting the hole component of the gate current measured at DC. Impact ionization occurs when electrons in the HEMT are accelerated in the high field region between the gated channel and the drain electrode. The electrons gain sufficient energy to ionize lattice atoms, creating free electrons and holes. The newly created electrons add to the drain current, while the holes are attracted to the gate, which is at a more negative potential than the drain. Measurements were carried out over a temperature range extending from 4K to 296K. DC measurements were made with an Agilent 4156C Semiconductor Parameter Analyzer with the devices placed in a Desert Cryo probing station to control the measurement temperature. At each temperature, gate and drain currents were measured while the gate voltage was stepped from -0.8V to +0.2 V in 0.1V increments and the drain voltage was stepped from 0.0V to 1.2 V in 0.05 V increments. The source was held at 0.0 V. The hole component of the gate current was extracted using the technique described in [1]. The hole current of a 0.15 μm x 40 μm AlGaAsSb/$In_{0.8}Ga_{0.2}As$ HEMT is plotted in Fig. 2 as a function of gate voltage at a drain bias of 1.2V. The characteristic bell shaped curve is evident at all temperatures. This shape occurs because at large negative gate voltages the channel is depleted and there are few carriers to participate in impact ionization, while at positive gate voltages, the electric field between the gate and the positively biased drain is decreasing, and impact ionization becomes less likely. At moderately negative gate voltages, these effects balance and a maximum hole current flows.

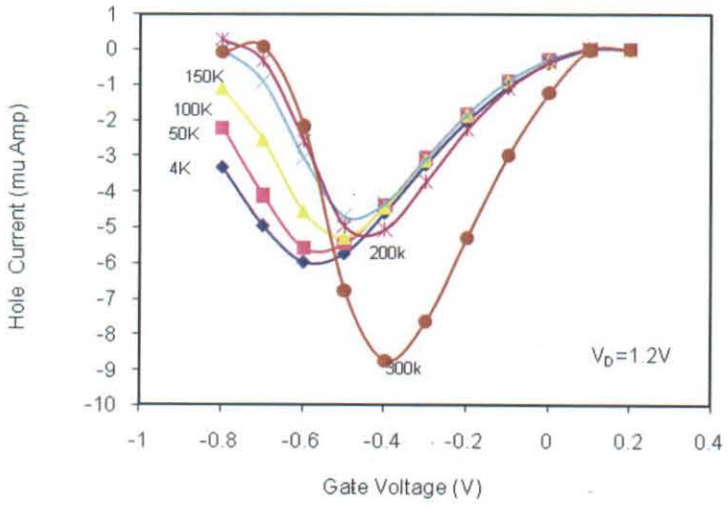

Figure 2: Extracted Hole Component of Gate Current versus Temperature

Fig. 3 shows the DC transconductance, g_D, as a function of gate to drain voltage. The onset of impact ionization occurs at a gate-drain voltage of 0.4 as evident from the dip in g_D. The

extraction of the ionization coefficient follows by plotting the log of the ratio of the hole component of the gate current to the drain current, I_{Hole}/I_D, as a function of reciprocal $(V_D-V_{D,sat})$ as shown in Fig. 4. Here, $V_{D,sat}$ is the drain voltage where the drain current saturates. The ionization coefficient is estimated from the intercept of the trend line (shown dashed for -0.7V) as $\alpha_n = \frac{1}{L} e^{Intercept}$, [1] where the length of the high field region, L, is estimated to be 0.5μm.

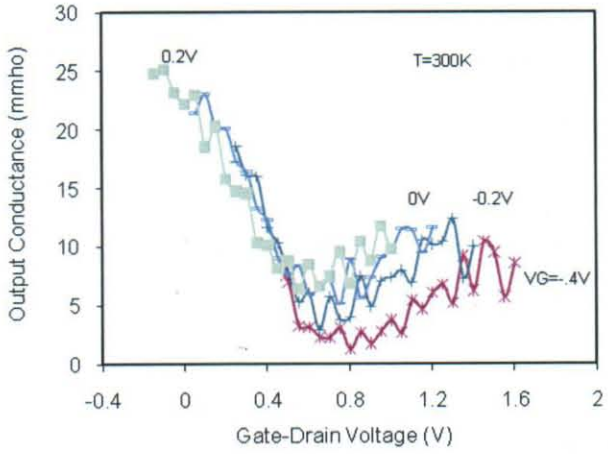

Figure 3: Room Temperature Output Conductance versus V_{GD}

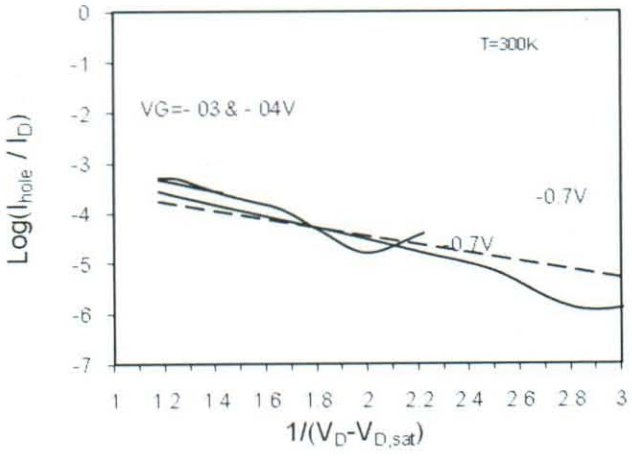

Figure 4: Log (I_{Hole}/I_D) versus Reciprocal ($V_D-V_{D,sat}$), Gate Bias as Parameter

The extracted electron ionization coefficient as a function of temperature is shown in Fig. 5. For gate voltages above threshold (>-0.7V) the initial increase in α at lower temperatures is believed to be due to limited scattering that allows electrons to absorb energy from the applied field

facilitating impact ionization. Fig. 5 is replotted as a function of V_G with temperature as a parameter in Fig. 6. The initial decrease in α at lower gate bias is due to the increase in effective band gap, defined as the separation of the eigen energies, resulting from the quantum well becoming more triangular with increasing 2DEG concentration. A journal article is in preparation for this work and will provide additional details on the analysis of this data.

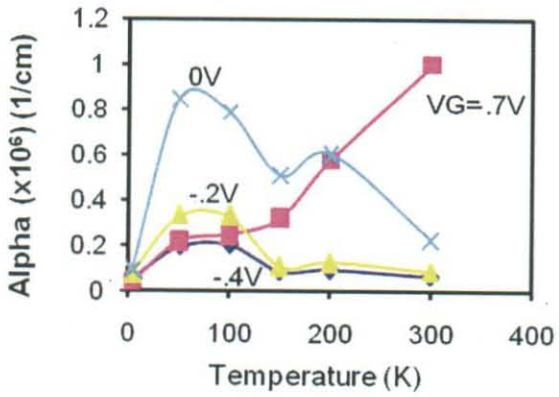

Figure 5: Impact Ionization Coefficient versus Temperature and V_G

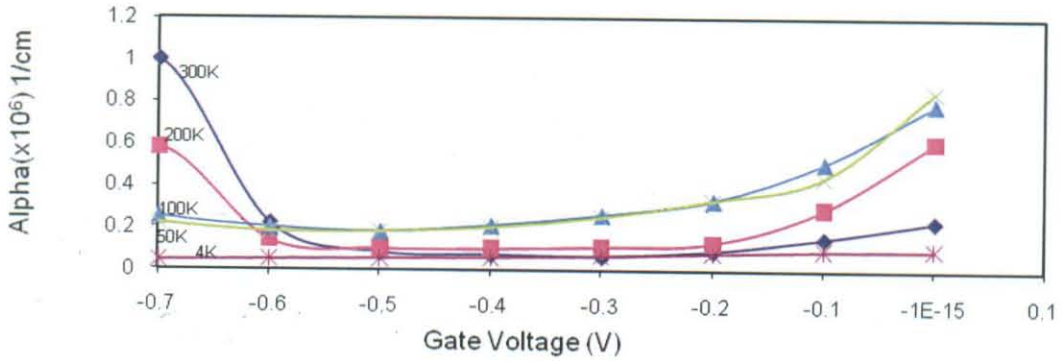

Figure 6: Impact Ionization Coefficient α versus VG and Temperature

Noise in AlGaAsSb/InGaAs/AlGaAsSb Metamorphic HEMTs (MHEMTs) was determined through measurement and physics based modeling. A minimum noise figure of 0.82 dB at 15 GHz obtained for 0.15 μm x 64 μm gates is an encouraging given the early stage of development for this material system. Additional details are available in [2].

3.3 GaN HEMTs

Initially, we examined the transport properties of GaN devices through physics based modeling. The Monte Carlo method was used to determine the electron mobility and diffusion constant in short GaN structures. Using the best available material parameters from the literature, the transport problem was set up, taking into account the scattering due to acoustic phonons, polar optical phonons, ionized impurities, impact ionization, alloy effects, interface effects with equivalent and non-equivalent inter-valley scattering. The Γ-L-X valleys were considered and assumed to be spherical. The simulation tracks about 20,000 electrons as they progress through the channel, with each electron suffering about 10,000 collisions. Channel length was varied from 0.1 μm to 2.0 μm. Velocity-field characteristics were compiled for each channel length over a field range from 0 to 1000 kV/cm. Mobility was determined from the slope of the velocity field characteristic at 20 kV/cm and is inversely proportional to channel length for lengths below 1 μm. In addition, the peak velocity moves to higher fields as the length decreases, that is the carriers become ballistic. Further details are available in [3].

We investigated the dependence of microwave performance of GaN/AlGaN High Electron Mobility Transistors (HEMTs), namely the unity gain current cut-off frequency (f_T) and the maximum oscillation frequency (f_{MAX}), as a function of the mole fraction of Al and the thickness of the barrier AlGaN layer [4]. The parameters were computed using a physics-based model and compared to experimental results. Schrödinger and Poisson's equations were solved self-consistently to relate the applied gate bias to the channel electron concentration. The contributions of both spontaneous and piezoelectric polarizations to f_T were explored. Finally, because of interest in using this family of devices at elevated temperatures, each simulation was repeated between 300K and 500K for comparison.

A mechanism for current collapse in GaN Metal Semiconductor Field Effect Transistors (MESFETs) was proposed, which assumed the existence of acceptor traps with multiple states in the bandgap. Current collapse has been experimentally observed in the current-voltage characteristic after the drain voltage sweep had exceeded the threshold for impact ionization in a previous measurement. In the proposed model, electrons generated by impact ionization are captured by neutral acceptor trap states in the substrate at energy levels above the valence band. The charged trap states move to an energy level located near midgap, creating a positively charged depletion region in the channel, and causing current collapse. With increasing drain bias, the quasi Fermi level approaches the charged trap states at the drain end of the gate, initiating detrapping of the electrons and restoring the current. The calculated results show good agreement with published experimental data. Further details are available in [5].

We investigated the gate bias dependence of the charge due to piezoelectric polarization in AlGaN/GaN HEMTs by implementing a fully coupled electro-mechanical formulation based upon the piezoelectric constitutive equations for stress and electric displacement. The coupled formulation results in lower charge due to piezoelectric polarization as compared to the

uncoupled formulation for a given Al-mole fraction. With increasing two-dimensional electron gas concentration, that is, for gate biases greater than threshold, the compressive strain along the c-axis in the barrier AlGaN layer increases with a concomitant increase of in-plane stress. We showed how current collapse correlates with the resulting increase in source and drain resistances through their dependence upon surface charge. We also formulated an alternate explanation of current collapse using local charge neutrality. This work was reported in [6].

To further investigate the current collapse phenomenon and to relate it to traps in the AlGaN/GaN HEMTs, we performed measurements of Transmission Line Method (TLM) structures. We can relate the pulse transient response of the TLM structures as a function of pulse rate and temperature to the energy levels and time constants of traps and potentially differentiate between effects occurring under the gate and effects occurring in the areas between the source, gate and drain contacts. Further details of this technique will be submitted for publication as a journal article.

A physics based model for GaN MESFETs was developed to determine the frequency dispersion of output resistance and transconductance due to traps. The equivalent circuit parameters were obtained by considering the physical mechanisms for current collapse and the associated trap dynamics. Detrapping time extracted from drain-lag measurements were 1.55 seconds and 58.42 seconds indicating trap levels at 0.69eV and 0.79eV, respectively. The dispersion frequency is in the range of MHz at elevated temperature, where a typical GaN power device may operate, although at room temperature it may be only a few Hz. For a 1.5 μm x 150 μm GaN MESFET with drain bias of 10 V and gate bias of -1V, 5% decrease in transconductance and 62% decrease in output resistance at RF frequencies from their DC values were observed. The dispersion characteristics were found to be bias dependent. A significant decrease in transconductance was observed when the device operated in the region where detrapping is significant. As gate bias approached cutoff, the difference in output resistance between DC and RF increases. For drain and gate biases of 10V and -5V, output resistance decreases from 60.2 K. at DC to 7.5 K. at RF for a 1.5 μm x 150 μm GaN MESFET. Further details are available in [7].

4.0 MICRO-ELECTRO-MECHANICAL SYSTEMS AND MICROMACHINED COMPONENTS

Radio Frequency Microelectromechanical Systems (RF MEMS) have generated a great deal of enthusiasm in the DOD community due to their potential impact on microwave and millimeterwave systems. RF MEMS switches have shown exceptional performance. In particular, these switches have a unique combination of low insertion loss (< 0.3 dB at 10 GHz), good isolation (> 20 dB at 10 GHz), low drive power (< 0.1 mW), wide-bandwidth (DC-60 GHz), and monolithic circuit integration. The impact of these switches in RF circuits is exemplified by their implementation in phase shifters. Phase shifters using RF MEMS switches

have been demonstrated from X-band through W-band. At every frequency, the MEMS based phase shifters have shown significantly lower loss than any other MMIC technology. The combination of exceptional RF performance, low drive power, and monolithic integration is not available from any other technology. This combination has direct impacts at the system level, particularly in the design of large-lightweight phased arrays.

However, when they were first introduced in the 1990's, RF MEMS switches were not viable for system implementation due to two key weaknesses: packaging and lifetime. These weaknesses severely impacted a number of DARPA programs including the MEMTenna, LCCMD, and Low Cost MEMS ESA programs. In all three cases the programs were terminated due to a lack of reliable MEMS switches. The lifetime of these switches is primarily driven by the physics of the contacting surfaces, and very long lifetimes can only be realized by a fundamental physical understanding of the contacting surfaces. The AFRL/RYHA basic research effort therfore focused on the problem of contact physics.

There are two primary types of RF MEMS switches: capacitive contact switches and metal contact switches. Capacitive contact switches are created by suspending a metal beam a short distance (typically 1-5 microns) above a dielectric coated lower metal. Applying a voltage between the two metals causes the suspended metal to collapse onto the dielectric, thus increasing the capacitance by a factor of 30-200, creating an effective short circuit at high frequencies. Metal contact switches remove the dielectric layer, and directly form a contact by driving one metal into the other. Our research investigated of the phenomena associated with bringing a metal surface into contact with either a dielectric or another metal.

4.1 Charging and Contact Physics in MEMS Switches

The primary focus of our work on capacitive contact switches was an investigation of dielectric charging. Capacitive switches operate by applying a large voltage between the two metal electrodes. This voltage pulls the suspended electrode down onto the dielectric. For most switches, the actuation voltage is on the order of 20-40 V. This voltage is dropped across the relatively thin dielectric (typically 0.2 micrometers) resulting in a field on the order of 10^8 V/m. Under such high fields, charge is injected into the dielectric where it becomes trapped and remains stored. To help us understand this mechanism, we performed simulations showing how charge in a thin film dielectric affects the performance of capacitive MEMS switches. The simulator incorporates fixed charge into the dielectric as a function of depth, and can readily be extended to handle charge as a function of both location and depth [8]. We validated these simulations with measurements from numerous switches. Direct observations of shifts in the Capacitance-Voltage (C-V) curves of capacitive switches correspond very well with our predictions. Using the measurement system created for verifying the C-V curve shift, we performed studies of charge build-up in the switches over extended cycling (up to 60 minutes) [9]. The data make it clear that the charging phenomenon is dynamic, with trapped charge concentration changing during the switch cycle.

We devised a new technique for measuring the voltage offset caused by charge in the dielectric layer of capacitive MEMS switches [10]. This technique does not require that the bridge come into contact with the dielectric. By avoiding contact during the measurements, the method measures the voltage shift caused by charge in the dielectric without introducing additional charge. Contact is avoided by driving the switch with a bias that always remains below the pull-in voltage. This low voltage results in only a small deflection of the bridge. The bridge deflection is dependent upon the applied bias and the charge in the dielectric. Although this deflection is small, it is sufficient to modulate a microwave signal. Therefore, by monitoring the modulated signal, the voltage shift can be directly observed. The technique is capable of measuring the charge induced-voltage shift with better than 0.2 V resolution.

An analytical calculation of microwave actuation for shunt capacitive MEMS switches was performed [11]. The calculation shows that the microwave signal deflects the beam according to the rms voltage of the signal. In addition, heating of the beam due to dissipated microwave power was shown to play a significant role in microwave actuation.

In metal contact switches, our efforts focused on understanding the metal-metal contact physics, in particular, the force versus voltage relationship for the switches. One of the primary design initiatives for metal-to-metal contact switches is to fabricate high force structures that exhibit low on-state contact resistances. Pull-in voltages can range from a few volts to 100 volts or more. The risk of having too low a pull-in voltage is that the beam can't provide enough restoring force to overcome contact forces and open the switch when the voltage is removed, thus the switch sticks closed. Too high a pull-in voltage causes difficulty in generating and distributing control voltages. With a high contact force, a better metal-to-metal contact is achieved which reduces the on-state resistance of the switch. For the metal contact switch, resistivity levels less than 1 ohm are desirable. An analysis of the contact and restoring forces for a series of metal contact micromechanical (MEMS) switches was performed. Several of the numerous tradeoffs required to increase contact and restoring forces were determined and reported in [12,13]. In collaboration with the Aerospace Components Division of the Sensors Directorate, we developed a new analytic contact resistance model for microswitches employing hemispherically-shaped upper contacts and sputtered contact metals [14]. The model was validated through the design, fabrication, and test of microswitches with metal alloy electric contacts. Overall, the results show increased microswitch reliability in exchange for a small increase in contact resistance for devices with bimetallic, binary alloy, and ternary alloy electric contacts.

In collaboration with the Air Force Institute of Technology, we investigated MEMS switch triboelectrification [15]. The goal of the work was to determine the degree of charge buildup due to the mechanical impingement of the switch onto the contacts and drive electrode. A dynamic model of switch deflection as a function of time was developed. This is a two-dimensional finite element beam model including electrostatic actuation. The model allows us to predict the bounce of the beam contact and the impact energy. We also developed a physics-based model of

charge injection resulting from the contact impacting the dielectric layer of the MEM actuating structure.

The residual stress and bending mechanisms in multi-layered nickel micro-cantilevers were examined through the use of interferometric microscope imaging. These cantilevers were constructed using layered, selective electrodeposition of Ni as a structural material and copper as the sacrificial material. Planarization of both the structural and sacrificial material occurs prior to subsequent layer depositions. Chemical etching of the sacrificial Cu layer is performed as a final step, releasing the structures. Each Ni deposition consists of a single layer of 8 μm thickness. The cantilevers were designed and fabricated with thicknesses ranging from 8 μm to 32 μm with corresponding lengths ranging from 200 μm to 500 μm. The cantilever array consisted of a series of 16 unique structures as illustrated in Fig. 7. Due to the planarization, these cantilevers had a near ideal fixed support instead of the typical stepped-up fixed support as generally observed in standard MEMS structures. In the four tested arrays, downward deflection was observed in all cantilevers. The measured downward deflection was most likely a result of either mismatch or the effects of planerization. Interpolation and error reduction techniques were used to account for sinusoidal variations in the interferometric measurements. Based on these data, analytic and computation approaches to the characterization of internal stresses were accomplished. Analytically, both pure bending and bending due to combined loading were considered in the characterization of the internal bending mechanisms and the calculation of the internal stress state. This behavior was examined as a function of both length and thickness. The Young's modulus used in the stress analysis was obtained from the cantilever fabricator, Microfabrica, Inc. Computationally, a finite element analysis software program (ANSYS, Ansys Inc.) was used to determine stresses resulting from an applied displacement equal to the maximum measured deflection. The result of this research on multi-layered Ni structures is important for both the successful design of RF MEMS components and for their performance. More specifically, this characterization enables the prediction of gaps, clearances, and behavior for electrostatically actuated devices.

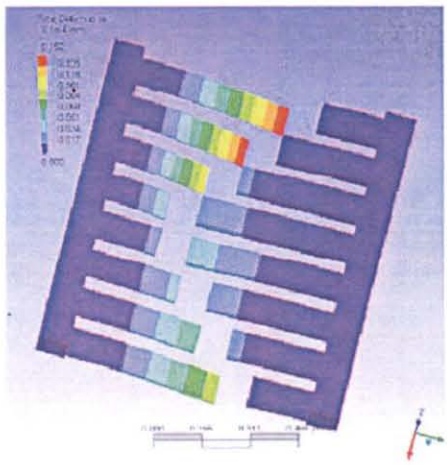

Figure 7: Deflection Model of Cantilever Array

4.2 New MEMS Devices and Packaging Concept

In addition to the studies of switch actuation and contacts, we researched new device and packaging concepts. A 2-bit digital variable MEMS capacitor was demonstrated with a capacitance range from 206 -335 fF [16]. The varactor consists of three cantilevered parallel plate capacitors. The bias voltage exerts electrostatic force to sequentially pull each cantilever down to a fixed stop, reducing the capacitor plate separation and increasing the capacitance. The cantilevers have different lengths and the longer ones collapse at lower voltage. Therefore, it can be biased with a single control voltage to allow simplified microwave system designs. The capacitor was designed so that the four capacitance states are approximately equally spaced. Fig. 8 shows a photomicrograph of the varactor and the measure capacitance-voltage curve. As a result of this work, United States patent number 7,283,347, *Low cost digital variable capacitor,* was issued October 16, 2007, with J. Robert Reid as the inventor.

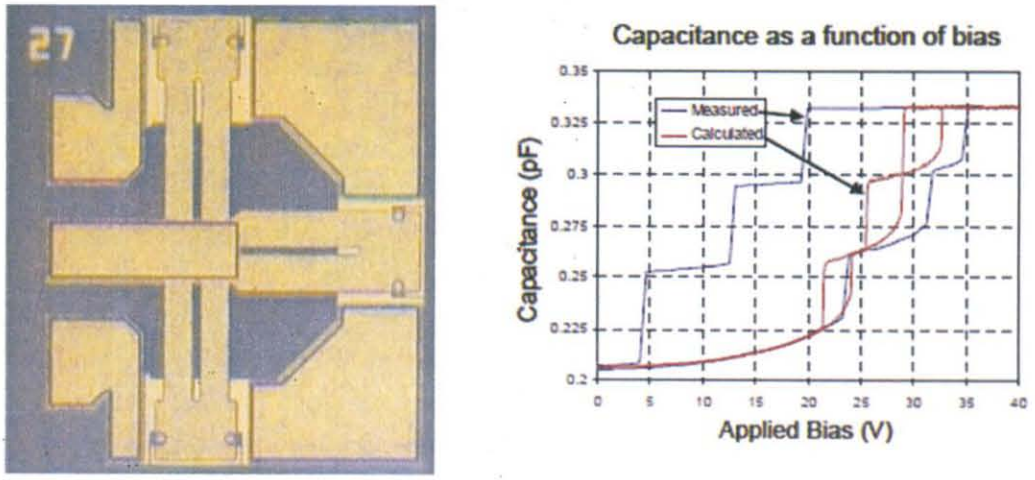

Figure 8: Optical Photo-micrograph of MEMS Varactor and Capacitance versus Applied Bias

We devised a method for contacting packaged MEMS switches that should result in higher performance, lower cost devices. Electrostatically actuated broadband micro-switches are prospective candidates as replacements for low-power mechanical relays or semiconductor switches and can be used in a variety of RF applications. These switches are fabricated using standard thin film processing allowing them to be integrated with active devices or designed into single-pole-single-throw (SPST), single-pole-double-throw (SPDT), or series-shunt switches. When compared with traditional electromechanical relays, MEMS RF switches provide significant savings in size and power consumption. However, as currently packaged, the individual switch die, shown in Fig. 9a, is fairly large at 1.45 mm square. Much of the topside area is required for making electrical contacts to the device. In addition, the cap projects above the contact pads by 0.4 mm.

With the new method, we gain access from the backside of the switch wafer to the metal contacts of the MEMS switch. In this manner, contact can be made under the glass frit, and the die size could be reduced to well under 1 mm square. In addition, the devices could easily be flip-chip bonded, allowing hybrid integration of the devices. To implement the process, the switches are fabricated using the existing commercial process, except that the silicon starting wafer is replaced by a silicon-on-insulator (SOI) wafer as shown in Fig. 9b. Using the buried SiO_2 layer as an etch stop, we remove most of the backside silicon wafer. Via holes can then be etched through the SiO_2, thin silicon, and oxide layers to make contact with the switch contacts under the glass wafer-bonding frit. This chip has shorter contact leads, lower contact parasitics, and is significantly smaller, so more chips can be fabricated on a wafer leading to lower cost per chip. We demonstrated this process on chips made by Radant MEMS, Inc on SOI wafers.

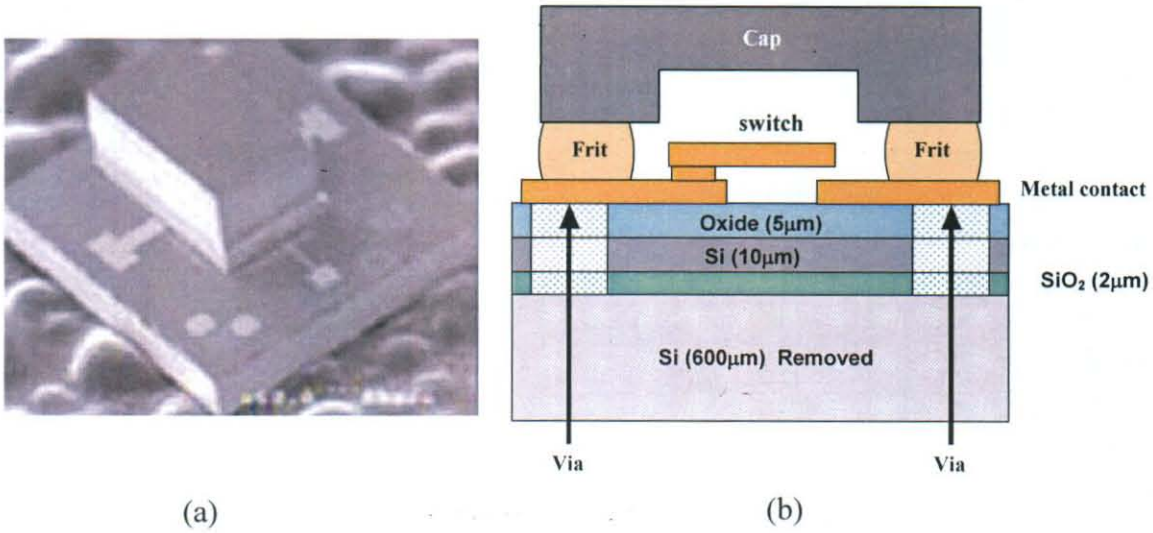

Figure 9: (a) SEM Micrograph of Commercial Capped Die Micro-switch (Radant MEMS, Inc.) (b) New Technique for Contacting Switch

4.3 Three Dimensional Millimeter-wave Components

We created innovative millimeter-wave components using emerging three-dimensional micro-fabrication technologies. Micro-fabrication allows greater precision, more flexibility, and better reproducibility than previous millimeter-wave circuit technologies. A key feature of the technology is that shielded transmission lines can be densely packed to form previously unrealizable, complex millimeter-wave networks. When mature, this technology will incorporate active and passive devices, radiating elements, and control circuitry, enabling fully integrated millimeter-wave sub-systems.

In our initial investigations, we built millimeter-wave components using a micro-fabrication technique being developed by Microfabrica, Inc. of Burbank CA. In this process, the following three steps are repeated to generate a desired number of metal layers: 1) A metal pattern is electroplated onto the substrate; 2) A second metal is blanket deposited over the entire substrate; 3) The top surface is planarized to create a single layer of uniform thickness with two metals. After all of the layers have been fabricated, one of the two metals is selectively etched away leaving the other metal in place to create 3D mechanical structures. The process is fundamentally the same as a sacrificial surface micromachining process, with two critical distinctions. First, the layers in this process are typically much thicker (2-15 μm) than in surface micromachining (0.5-4 μm). Second, the planarization allows significantly more layers (>> 10) than are common in surface micromachining. Fig. 10a shows a three dimensional shielded coaxial line with a coplanar transition for millimeter-wave probing. The metal structure is 92 μm high, and consists of twelve layers of nickel on an alumina substrate.

As an example of the excellent millimeterwave performance we achieved on our first build, Fig. 10b shows a 60 GHz branch line coupler fabricated using the rectangular coaxial transmission lines [17]. The coupler has a measured insertion loss of 3.4-4.2 dB over the 55-61 GHz frequency range. The device was fabricated successfully in a single design pass. We also built a V-band bandpass filter. The use of integrated coaxial lines allows the fabrication of a compact filter measuring 6.5 mm x 2.0 mm x 0.1 mm. In addition, the coaxial lines isolate the filter from the external environment allowing filters to be spaced close to other devices without electromagnetic coupling. The fabricated filter has a center frequency of 57.5 GHz and a bandwidth of 2.5 GHz [18]. We transitioned this 3D component work to exploratory development, and continue to develop advanced components including switch matrices, tunable filters, and diplexers.

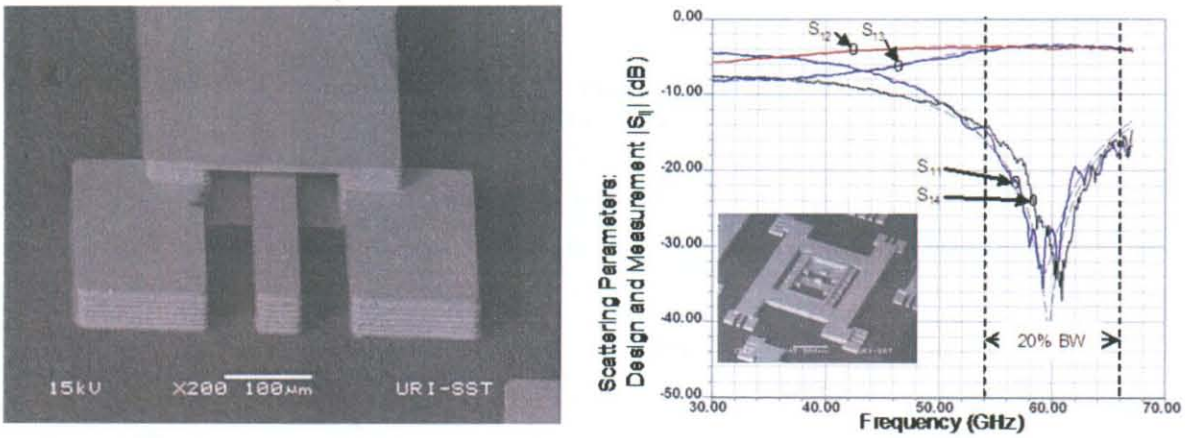

(a) (b)

Figure 10: a) Three-dimensional Millimeter-wave Coaxial Line with Coplanar Transition for Probing (b) 60 GHz Branch Line Coupler, Measured S-parameters Agree with Design Curves

5.0 EMERGING MATERIALS FOR ELECTROMAGNETIC COMPONENTS

5.1 Thin Film Pyroelectrics

Pyroelectric materials produce a voltage that is proportional to the change in temperature and a room temperature sensor of millimeterwaves can be made from pyroelectric thin films. We investigated AlN as a candidate for pyroelectric sensors. We prepared thin films of AlN by DC reactive sputtering of aluminum in $3x10^{-3}$ Torr ammonia atmosphere onto polished n-type silicon wafers. The power density at the target was approximately 5 Watts cm^{-2}. The substrates were 0.1 Ω-cm, n-type polished silicon with (111) orientation. The films were heated to above 200 C and cooled to <50 C with the chamber at or below $1x10^{-8}$ Torr prior to the sputter deposition. The resulting AlN films were semi insulating to slightly p-type with typical through-film resistance of 25MΩ/μm for 1 cm^2 of area. The thickness of films thus prepared, varied in the range 600 Å to 2500 Å controlled by sputtering time. Subsequent to the AlN deposition, a 400 Å layer of NiCr was applied to act as both a contact to the AlN and to increase the infrared (IR) absorbance. The n-type silicon substrate was used as the back contact. To measure the pyroelectric response, a broadband incident source was focused on the specimen after passing through a vane chopper. A silicon wafer etched and polished on both sides was interposed between the source and the specimen to insure that any electrical responses related to the AlN/Si substrate interface were suppressed. Response of a specimen to the chopped IR source is given in Fig. 11. As expected for a pyroelectric material, the AlN film responds only to the time rate of change of temperature (dT/dt) rather that to the absolute value of temperature per se. A first estimate of response time can be obtained from the exponential decay part of the trace. The roll-off part of the data rise was fitted to an exponential as shown in Fig. 12. From that a 1/e response time of 0.013s is calculated. If one assumes a linear rise in temperature proportional to the rate of energy input and an exponential fall off proportional to the conductivity of the AlN and the Si substrate on which it was formed, then the time to maximum temperature rate of change is 0.75s, which is close to the value observed in the figure. Additional information on this pyroelectric AlN work can be found in [19].

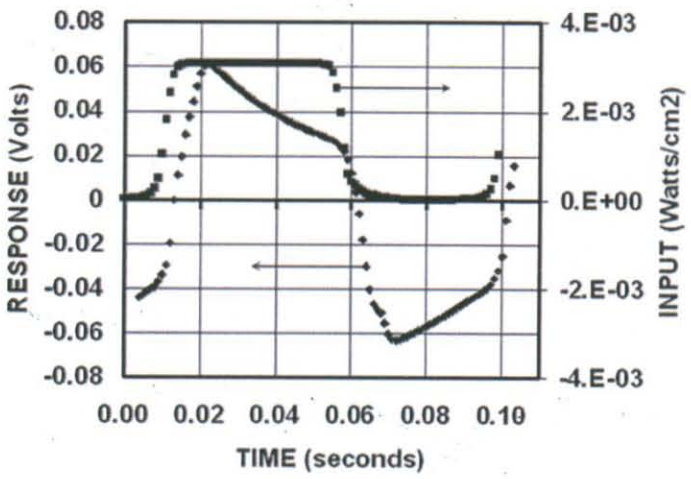

Figure 11: Response of AlN Film to Pulsed, Broadband, IR Light

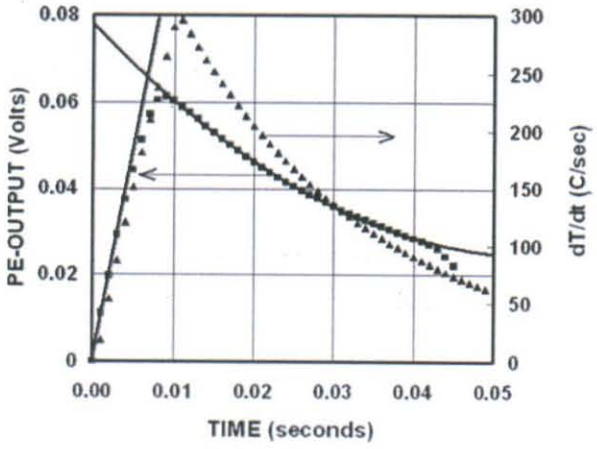

Figure 12: Positive Response Half Cycle of Fig. 11 compared to Rate of Temperature Change from Heat Transfer Model

5.2 Polymer Materials for Tunable Microwave Devices

Previous experience with polymer compounds indicate that poly (vinylidene) fluoride (PVDF) might be an appropriate candidate for creating tunable microwave devices such as phase shifters, time delay units, and reconfigurable antennas. We chose PVDF to investigate as the starting material because it is a well-documented polymer, extremely durable in solid form, readily dissolved, ultraviolet radiation resistant, and shown by researchers to have complicated polymorphism properties. Fig. 13 shows a model of PVDF created in the atomic chemical bonding computational computer graphics program HyperChem7.

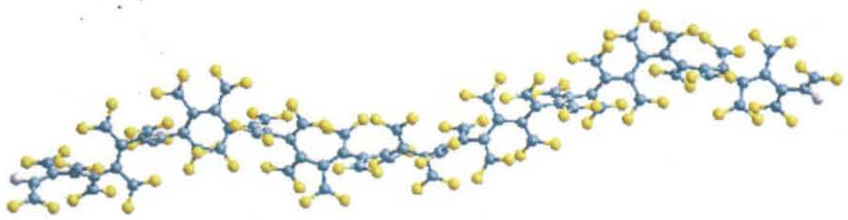

Figure 13: PVDF Alpha-Phase Model, Carbon = blue; Hydrogen = white; Fluorine = yellow

PVDF is a piezoelectric material. This means that when it is placed in an electric field it will change shape. Because fluorine is so much more electronegative than carbon, research has demonstrated that the fluorine atoms pull electrons away from the carbon atoms. This makes the CF_2 groups polar, with a partial negative charge on the fluorine atoms and a partial positive charge on the carbon atoms. When we place the molecule in an electrical field, the electrons will align causing the polymer sample to deform. It is already known that one of the polymorphs of PVDF (β-phase) is strongly ferroelectric. In consultation with Prof. William Euler, polymer expert from the University of Rhode Island, we explored ways to incorporate magnetic ions, such as cobalt and manganese, into to PVDF structure.

Solid PVDF-plus-ion specimens were prepared by retarded evaporation of the solvent from a quantity of solution contained in small ampoule bottles. Solidification was effected with and without the presence of polarizing 3 kG permanent magnets adjacent to the solidification chamber. Several chambers were constructed for specimen preparation including chambers that permit compressive stress to be applied after solidification. The specimens thus prepared were then measured in a SQUID magnetometer to determine their magnetic signature. Several specimens showed ferromagnetic response. In particular, the ones prepared from cobalt-based salts showed both the saturation and hysteresis character of ferromagnetic material. These were analyzed for optical transmission. Specimens of PVDF with gadolinium as the magnetic ion were also prepared for optical analysis. Because of the strong color tints of the liquid PVDF-plus-ion solutions, particularly when Co ions were used, the liquids were analyzed in the visible through near IR (380-1200nm). Strong absorption of the solvents precluded extending the measurements any further into the IR.

Thin films of the solutions were prepared by spinning onto 4 inch diameter polished silicon wafers. While the parameters necessary for consistent film production (spin speed, solution viscosity, and temperature) were not fully determined, portions of the films were measured by Fourier Transform Infrared spectroscopy (FTIR) and some interesting trends were observed. The following preliminary conclusions were drawn from our analyses:

1. The presence of the magnetic ions, regardless of specie, promotes the formation of the polar beta phase as opposed to the alpha phase that is usually more prevalent with the spin-casting and retarded evaporation methods of PVDF thin film preparation.

2. The largest magnetization effect observed was in a Co 'doped' specimen that contained 0.08% weight percent.

3. Both Gd and Mg containing PVDF specimens showed minimal magnetization response.

4. The IR transmission measurements are suitable for determining the ratios of the PVDF phases commonly formed by our preparation methods.

5. Scanning Electron Microscope/Electron Diffraction Spectroscopy (SEM/EDS) measurements of several films disclosed that the magnetic ion species (M+) are generally evenly distributed throughout the PVDF specimens. Occasionally, in the specimens with the highest concentrations, islands of concentrated M+ were observed, but such localization did not show correlation with the SQUID response.

For microwave measurements, we prepared pellets with a diameter that is slightly larger than the coaxial waveguide used to measure permeability and permittivity of the materials. Final fit to the waveguide was performed by miniature lathe machining of the pellets. Measurements and analysis of PVDF-plus-Co specimens in the coaxial waveguide showed regions of reduced permeability ($\mu<1$) centered at 13.6 GHz. This frequency is quite close to the reported value for electron paramagnetic resonance (EPR) of Co. However, deconvolution of the permittivity and permeability parameters from our preliminary measurements proved to be quite complex because of the extensive procedures required to calibrate the wave guide system for particular wave length regions. Thus, the correctness of these values is suspect. Our intent was to continue this work under a new research task, but that task has not been funded.

5.3 Nanowire Formation

We investigated the potential of reactive sputtering as a process for creating III-N nanowires. Simple reactive sputtering forms uniform, smooth, high density, polycrystalline films with c-axis orientation normal to the surface of the substrate. To promote filament growth out of the plane of the film growth, we added a driving force in the form of a high voltage negative bias onto the substrate with respect to the plasma. Typical temperature for growth is 350°C. We performed the experiment on silicon substrates with ~100Å of either SiO_2 or Al_2O_3 on the growth side of the substrate. Seeding of nanowires was promoted by depositing ~50Å gold layer on top of the SiO_2 or Al_2O_3 and then heating to 700°C. This processing uses to advantage the low wetting coefficient of the Au/oxide interface causing the Au to form submicron (nearly) circular dots which then act as the seed points for filament growth. The process was applied to the growth of GaN. Using -1000 V_{DC} bias, areas of filament growth were regularly formed. Both rod-like and articulated growths were observed but the processing parameters that control the various

morphologies are not understood as yet. The fact that neither unbiased nor positively biased substrates show any sign of filaments on their surfaces demonstrates that the negative bias field is important for III-N nanorod growth. Fig. 14 shows some examples of growth morphologies observed for the field enhanced reactive sputtering of GaN. On the left are commonly observed articulated loops. The largest loop in the picture is approximately 60μm long. In the center is a straight rod in proximity to an articulated loop. On the right is an example of pathological growth formation. In most of the growths the bright and/or bulbous end of the filament represents the Au seed from which the filament growth proceeds.

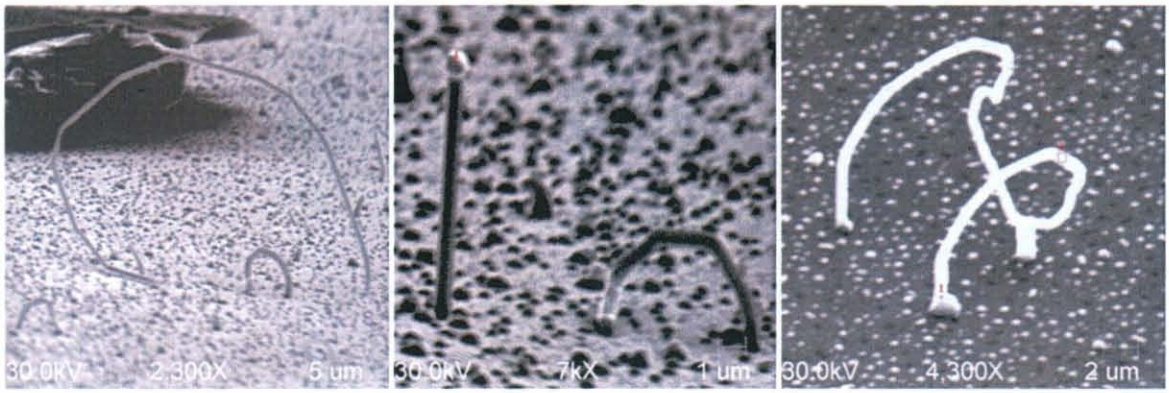

Figure 14: Examples of GaN Nanowires

6.0 NOVEL SENSORS

6.1 Optical Strain Gages

We performed experiments and analysis of bending strain sensors based on hollow wave-guide capillary coated with optically active thin films. The strain sensors were designed for compatibility with optical fiber installations and can be attached to structures to measure their bending strains. The sensors can be adjusted to maximize gage factor for predetermined strain ranges. The sensor consists of glass micro tubing coated on the outer surfaces with an optical absorbing layer followed by a reflecting layer. A mechanical strengthening layer was included in some experiments to extend the measurable range of strain. In operation, a source laser beam from an optical fiber is injected into one end of the gage. The light remaining in the beam after traveling through the gage is collected via another optical fiber. For a given thickness of the absorber layer, the detected light is proportional to the amount of bending. Thus by rigidly affixing the sensor to a structural member, the instantaneous strain and strain history experienced by the member can be monitored. Typical gage lengths are 3 to 10 cm. Applications envisioned for this device include monitoring the strain histories of buildings in earthquake prone areas,

ships on the open seas and airplanes during abrupt maneuvers. Several specimens where constructed with differing silicon layer thickness as the optically absorbing layer. Gage factors from -40 to -200 were measured for those specimens with the absolute value increasing as the thickness of the silicon absorber was increased. Maximum strains of 5000 micro-strain where observed for the gages prepared on bare glass capillaries. The maximum observable strain was increased to 10,000 micro-strain by the addition of a one micrometer thick polyamide strengthening coating on the capillary. This research project resulted in United States patent number 7,002,673, *Optical strain gage compatible with fiber optic systems*, E. E. Crisman, inventor.

6.2 Micro-machined millimeter-wave sensors

We combined MEMS micromachining with thin film technology as a step toward creating a simple low cost millimeter-wave sensor. The sensor consists of a planar millimeter-wave dipole antenna, terminated by a thin film resistor, thermally isolated from the underlying substrate by micromachining. Energy received by the antenna is dissipated in the resistor causing the resistor's temperature to rise. In our initial work, the change in temperature was measured using a thermopile. Thermal and millimeter-wave radiation calculations showed there is potential for the sensor to work actively and passively in an outside environment. We used the MOSIS fabrication service as an economical way to make the antenna, resistor, and interconnect circuitry. This is a standard CMOS process that we adapted to create millimeter wave antenna elements, resistors, thermopiles, and patterned glass structures for subsequent etching in our clean room. On the fabrication runs, we included test structures for each of these components as well as prototype sensors. A millimeter-wave antenna and a dc test structure are shown in Fig. 15a and 15b. The DC test results in Fig. 15c showed sensitivities in the range of 10 to 14 mV/mW. However, the sensitivity of the 94 GHz sensor was low due to interaction with the underlying silicon that was not properly accounted for in the initial design. We developed a process for release-etching the suspended structures using an initial etch in XeF_2 followed by a Tetra Methyl Ammonium Hydroxide (TMAH) wet etch which selectively removes silicon but not glass. The process includes a method for mounting the die to prevent backside etching. This work will continue under a new research task, using pyroelectric material as the temperature sensing element.

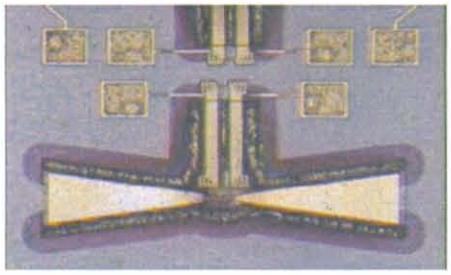

(a)

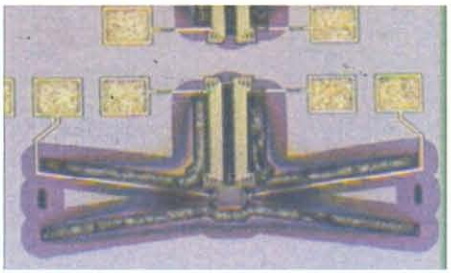

(b)

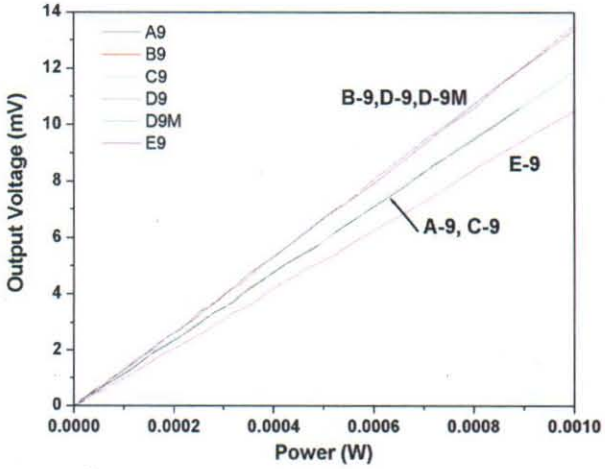

(c)

Figure 15: (a) 94 GHz Antenna Feeds Suspended Resistor (b) Thermopile Test Structure (c) Thermopile DC Voltage-Power Response

6.3 Micro-Robots

We envision the creation of autonomous robotic sensors for close-in and surface detection of physical and chemical phenomena. Our specific objective in this research was to provide proof of principle for three dimensional Silicon-On-Insulator (3D SOI) micro-spheres as a platform for autonomous sensors. Ultimately the devices would include a sensing mechanism, a means for autonomous motion, communication and control electronics, and a power source. With the help of advances that others are making in the theory and practice of robotics, these autonomous robots can act in ensembles, communicating with each other and with higher levels of the sensor network.

As they mature, the micro-sensors could detect a variety of phenomena including acoustic, electromagnetic activity, motion, and biological or chemical agents. Their sub-cubic-millimeter volume is significantly smaller than sensors in current practice. The small size means they can be deployed covertly or in highly confined or dangerous spaces such as building rubble. Since the sensors would be batch produced using semiconductor processing techniques, they should be very low cost.

The use of a large number of low cost, autonomous sensors acting as an ensemble is a significant change from the current practice, wherein a small number of sophisticated, high value sensors are used to detect or monitor phenomena. Although the current practice is effective and will

remain so in the future for many functions, the autonomous microsensor would provide an additional capability for covert, constricted, or dangerous environments.

Our research showed that we can use built-in layer stress to form micro-spherical shells of silicon sandwiched between oxide layers. We demonstrated a process for fabricating spheres and developed formulas for predicting the 3D shape based on the material properties. Fig. 16 shows scanning electron micrographs of spherical shells formed from silicon and oxide layers. The shell in Fig. 16a has a diameter of approximately 1 mm and was formed from a two dimensional flower pattern. A close up of a hemispherical structure showing the central hub is shown in Fig. 16b. Fig 16c shows a top view of an approximately 1.1 mm diameter shell formed with ribs to cover additional area. We demonstrated controlled motion of the spheres using a pattern of external electrodes excited by voltage pulses. Our analysis showed that we can incorporate electronics in the embedded silicon and supplement that with hybrid components enclosed within the 3D structure. Analysis further showed that we can provide and store enough power for sensing, computation, communication, and actuation, and that power dissipation will not have adverse thermal effects. We consulted experts in ensemble robotics who are convinced that sufficient computational capability can be incorporated in the 3D structure within the expected power and thermal budgets.

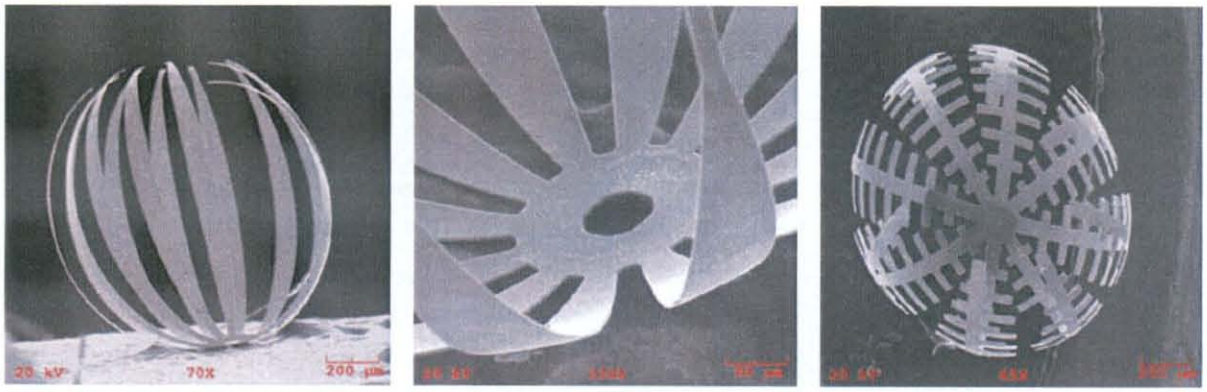

(a) (b) (c)

Figure 16: Scanning Electron Micrographs of Spherical Shells (a) Approx. 1 mm Diameter Shell (b) Close up of Hemispherical Structure (c) Approx. 1.1 mm Diameter Shell

The successful development of autonomous microsensors will provide a sensing capability that is not available today. An ensemble of small, low cost, expendable sensors that can be dispersed and maneuvered offers unique opportunity to increase situational awareness. The microsensors could give decision makers data on diverse phenomena such as the presence or movement of individuals or vehicles; the presence of explosive, chemical, or biological agents; the presence

and content of conversations or electromagnetic emissions. After our initial success with micro-robots, future work in this area will be performed under a separately funded research task.

7.0 CONLCUSIONS AND RECOMMENDATIONS

The broad objective of the Electromagnetic Component Research task was to improve our fundamental understanding of phenomena that enable or limit the future development of electromagnetic components for antenna applications. This objective was met through the investigation of a number of technical areas including semiconductor device physics, RF MEMS devices, 3D integrated circuits, multi-ferroic polymer materials for tunable RF components, nanowire formation, novel sensor components, and micro-robotics.

The research effort produced thirty-six publications, three patents, and large number of invited and contributed presentations. Several research areas have been transitioned to exploratory development, in particular, the MEMS and 3D circuit work.

Two areas have been recommended for continuation and will be funded under new research tasks. The *Ensemble Based Matter* task will explore the creation and physics of dynamic matter formed from an ensemble of coordinated of sub-cubic millimeter robots. *Antenna-Coupled Millimeter-Wave Detectors using Pyroelectric Thin Films* will research a sensor consisting of an antenna, resistive load, pyroelectric capacitor, and interconnects supported by a micromachined silicon dioxide membrane on a silicon substrate.

REFERENCES

1. Webster, R. T., Wu, S., and Anwar, A. F. M., "Impact Ionization in InAlAs/InGaAs/InAlAs HEMTs," IEEE Electron Device Letters, Vol. 21, No. 5, pp 1930195, May 2000.
2. Webster, R. T., and Anwar, A. F. M., "Noise in Metamorphic AlGaAsSb/ InGaAs/ AlGaAsSb HEMTs," Solid State Electronics, vol. 48, pp 2007-2011, Oct 2004.
3. Anwar, A. F. M., Wu, S., and Webster, R. T., "Temperature Dependent Transport Parameters in Short GaN Structures" phys. stat. sol. (b), Vol.288, No.2, pp 575-578, 2001.
4. Anwar, A. F. M., Wu, S., and Webster, R. T., " Temperature Dependent Transport Parameters in Short GaN Structures," Proceedings of the 4th International Conference on Nitride Semiconductors – Part B, Fernando A. Ponce and Abigail Bell (Eds.), pp 575-578, December 2001.
5. Anwar, A. F. M., Islam, S. S., and Webster, R. T., "Carrier trapping and Current Collapse Mechanism in GaN metal semiconductor field effect transistors," Applied Physics Letters, Vol. 84, No. 11, March 2004.
6. Anwar, A. F. M., Webster, R. T., and Smith, K. V., "Bias induced strain in AlGaN/GaN heterojunction field effect transistors and its implications," Applied Physics Letters, Vol.88, 19 May 2006.
7. Islam, S. S., Anwar, A. F. M., and Webster, R. T., "A Physics Based Frequency Dispersion Model of GaN MESFETs," IEEE Transactions on Electron Devices, Vol.51, No.6, pp 846-853, June 2004.
8. Reid, J. R., "Simulation and Measurement of Dielectric Charging in Electrostatically Actuated Capacitive Microwave Switches", Modeling and Simulation of Microstructures (MSM 2002), San Juan, PR, April 2002.
9. Reid, J. R. and Webster, R. T., "Measurements of Charging in Capacitive Microelectromechanical Switches," IEE Electronics Letters, Vol. 38, No. 24, 21 Nov. 2001.
10. Reid, J. R., Webster, R. T., and Starman, L. A., "Non-Contact Measurement of Charge Induced Voltage Shift in Capacitive MEM-Switches," Microwave and Wireless Components Letters, Vol.13, No. 9, p 367, Sept. 2003.
11. Reid, J. R., Starman, L. A., and Webster, R. T., "RF Actuation of Capacitive MEMS Switches," in *IEEE Microwave Theory and Techniques Symposium Digest of Papers*, June 2003.

12. Coutu Jr., R. A., Starman, L. A., Reid, J. R., and Kladitis, P.E., "Finite Element Modeling and Simulation of Micro-Switch Pull-in Voltage and Contact Force," in *Eurosensors*, September 2003.
13. Reid, J. R. and Starman, L. A., "Simulation of cantilever beam micro-switch pull-in and collapse voltages," in *Proceeding of the Sixth International Conference on Modeling and Simulation of Microsystems*, MSM 2003, February 2003.
14. Coutu, R.A. , Reid, J. R., Cortez, R., Strawser, R.E., and Kladitis, P.E., "Microswitched with Sputtered Au, AuPd, Au-on-AuPt, and AuPtCu Alloy Electrical Contacts," IEEE Transactions on Components and Packaging Technologies, Vol. 29, No. 2, pp 341-349, June 2006.
15. Coutu, R.A., Kladitis, P.E., Starman, L. A., and Reid, J. R., "A comparison of micro-switch analytic, finite element, and experimental results," Sensors and Actuators A: Physical, Vol. 115, pp 252-258, 2004.
16. Reid, J. R., Starman, L. A., and Webster, R. T., "4-State Digital Variable Capacitors," EuroSensors XVIII Technical Digest, September 2004.
17. Reid, J. R. and Webster, R. T., "A 60 GHz Branch Line Coupler Fabricated Using Integrated Rectangular Coaxial Lines," IEEE International Microwave Symposium Digest, June 2004.
18. J. R. Reid and Webster, R. T., "A Compact Integrated Coaxial V-Band Bandpass Filter," IEEE International Antennas and Propagation Symposium Digest, June 2004.
19. Crisman, E. E., Derov, J. S., Drehman, A. J., Gregory, O. J. "Large Pyroelectric Response from Reactively Sputtered Aluminum Nitride Thin Films," Electrochemical and Solid-State Letters, Vol. 8 No. 3, pp H31-H32 2005.

APPENDIX -PUBLICATIONS, PATENTS, AND PRESENTATIONS

Archival Journal Publications

1. A. F. M. Anwar, Shangli Wu, and Richard T. Webster, "Temperature Dependent Transport Parameters in Short GaN Structures" phys. stat. sol. (b), Vol.288, No.2, pp 575-578, 2001.
2. J.R. Reid and R.T. Webster, "Measurements of Charging in Capacitive Microelectromechanical Switches," IEE Electronics Letters, Vol. 38, No. 24, 21 Nov. 2001.
3. J.R. Reid, R.T. Webster, and L.A. Starman, "Non-Contact Measurement of Charge Induced Voltage Shift in Capacitive MEM-Switches," Microwave and Wireless Components Letters, Vol.13, No. 9, p 367, Sept. 2003.
4. R. T. Webster and A. F. M Anwar, "Noise in Metamorphic AlGaAsSb/ InGaAs/ AlGaAsSb HEMTs," Solid State Electronics, Vol. 48, pp 2007-2011, Oct 2004.
5. S. S. Islam, A. F. M. Anwar, and R. T. Webster, "A Physics Based Frequency Dispersion Model of GaN MESFETs," IEEE Transactions on Electron Devices, Vol.51, No.6, pp 846-853, June 2004.
6. A. F. M. Anwar, S. S. Islam, and R. T. Webster, "Carrier trapping and Current Collapse Mechanism in GaN metal semiconductor field effect transistors," Applied Physics Letters, Vol. 84, No. 11, March 2004.
7. E. Faraclas, R. T. Webster, G. Brandes, and A. F. M. Anwar, "Dependence of RF Performance of GaN/AlGaN HEMTs upon AlGaN Barrier Layer Variation," International Journal of High Speed Electronics and Systems, Vol.14, No. 3, pp 750-755, 2004.
8. R.A. Coutu, P.E. Kladitis, L.A. Starman, and J.R. Reid, "A comparison of micro-switch analytic, finite element, and experimental results," Sensors and Actuators A: Physical, Vol. 115, pp 252-258, 2004.
9. E. E. Crisman, J. S. Derov, A. J. Drehman, O. J. Gregory, "Large Pyroelectric Response from Reactively Sputtered Aluminum Nitride Thin Films," Electrochemical and Solid-State Letters, Vol. 8 No. 3, pp H31-H32 2005.
10. J.F. Kucko, J.C. Petrosky, J.R. Reid, and Y.K. Yeo, "Non-Charge Related Mechanism Affecting Capacitive MEMS Switch Lifetime," IEEE Microwave and Wireless Components Letters, Vol. 16, No. 3, pp 140-142, March 2006.
11. A. F. M. Anwar, R T. Webster, and K. V. Smith, "Bias induced strain in AlGaN/GaN heterojunction field effect transistors and its implications," Applied Physics Letters, Vol.88, 19 May 2006.

11. A. F. M. Anwar, R T. Webster, and K. V. Smith, "Bias induced strain in AlGaN/GaN heterojunction field effect transistors and its implications," Applied Physics Letters, Vol.88, 19 May 2006.
12. R.A. Coutu, J.R. Reid, R. Cortez, R.E. Strawser, and P.E. Kladitis, "Microswitched with Sputtered Au, AuPd, Au-on-AuPt, and AuPtCu Alloy Electrical Contacts," IEEE Transactions on Components and Packaging Technologies, Vol. 29, No. 2, pp 341-349, June 2006.
13. J. R. Reid, E. D. Marsh, and R. T. Webster, "Micromachined Rectangular Coaxial Transmission Lines," IEEE Transactions on Microwave Theory and Techniques, Vol. 54, No. 8, pp3433-3442, Aug 2006.
14. E. D. Marsh, J. R. Reid, and V. S. Vasilyev, "Gold-Plated Micromachined Millimeter-Wave Resonators Based on Rectangular Coaxial Transmission Lines," IEEE Transactions on Microwave Theory and Techniques, Vol. 55, No. 1, pp 78-84, Jan 2007.

Conference Proceedings Papers

1. J.R. Reid, "Capacitive Switch Reliability Issues", in GOMAC, Monterey, CA, March, 2002.
2. J.R. Reid, "Simulation and Measurement of Dielectric Charging in Electrostatically Actuated Capacitive Microwave Switches", Modeling and Simulation of Microstructures (MSM 2002), San Juan, PR, April 2002.
3. A. F. M. Anwar, Shangli Wu and R. T. Webster," Temperature Dependent Transport Parameters in Short GaN Structures," Proceedings of the 4th International Conference on Nitride Semiconductors – Part B, Fernando A. Ponce and Abigail Bell (Eds.), p 575-578, December 2001.
4. R.A. Coutu Jr., L.A. Starman, J.R. Reid, and P.E. Kladitis, "Finite Element Modeling and Simulation of Micro-Switch Pull-in Voltage and Contact Force," in *Eurosensors*, September 2003.
5. J.R. Reid and L. Starman, "Simulation of cantilever beam micro-switch pull-in and collapse voltages," in *Proceeding of the Sixth International Conference on Modeling and Simulation of Microsystems*, MSM 2003, February 2003.
6. J.R. Reid, L.A. Starman, and R.T. Webster, "RF Actuation of Capacitive MEMS Switches," in *IEEE Microwave Theory and Techniques Symposium Digest of Papers*, June 2003.
7. Syed S. Islam, A. F. M. Anwar and Richard T. Webster, "A physics-based model of frequency-dependent characteristics of GaN MESFETs," 2003 Device Research Conference, Salt lake City, Utah, 2003.
8. J.R. Reid, L.A. Starman, and R.T. Webster, "4-State Digital Variable Capacitors," EuroSensors XVIII Technical Digest, September 2004.

9. R. T. Webster and A. F. M. Anwar, "Temperature Dependence of Impact Ionization in AlGaAsSb/InGaAs/AlGaAsSb Metamorphic HEMTs," 2004 IEEE Lester Eastman Conference on High Performance Devices, pp 83-84, August 2004.
10. E. W. Faraclas, R. T. Webster, G. Brandes, and A. F. M. Anwar, "Dependence of RF Performance of GaN/AlGaN HEMTs upon Barrier AlGaN Layer Thickness and Mole Fraction Variation," 2004 IEEE Lester Eastman Conference on High Performance Devices, pp 63-64, August 2004.
11. J. R. Reid and R. T. Webster, "A Compact Integrated Coaxial V-Band Bandpass Filter," IEEE International Antennas and Propagation Symposium Digest, June 2004.
12. J. R. Reid and R. T. Webster, "A 60 GHz Branch Line Coupler Fabricated Using Integrated Rectangular Coaxial Lines," IEEE International Microwave Symposium Digest, June 2004.
13. L. A. Starman, J. R. Reid, R. T. Webster, and J. L. Ebel, "RF MEMS Switches for Antenna Applications," International Symposium for MEMS and Nanotechnology Proceedings, June 2004.
14. R. A. Coutu, P. E. Kladitis, L. A. Starman, and R. L. Crane. "RF MEMS Switches with Metal Alloy Electric Contacts," Proc. 2004 Solid-State Sensor, Actuator, and Microsystems Workshop at Hilton Head, 188–191, June 2004.
15. R T. Webster, J. R. Reid, and L. A. Starman, "RF MEMS Metal Contact Switch: Design, Measurement and Modeling," IEEE Wireless and Microwave Conference Proceedings, April 2004.
16. J.R. Reid, R.T. Webster, and E.D. Marsh, "Micromachined Coaxial Transmission Lines," TEXMEMS VII, September 2005.
17. J. R. Reid and R. T. Webster, "A 55 GHz Bandpass Filter realized with Integrated TEM Transmission Lines," International Microwave Symposium Digest, June 2006.
18. J. R. Reid and R. T. Webster, "A 6-port 60 GHz Coupler for an RN2 Beam Former," IEEE International Antennas and Propagation Symposium Digest, June 2006.
19. J. R. Reid, D Hanna, and R. T. Webster, "A 40/50 GHz Diplexer Realized with Three Dimensional Copper Micromachining," IEEE International Microwave Symposium Digest, June 2008.
20. J.R. Reid, V.S. Vasilyev, and R.T. Webster, "Building Micro-Robots: A Path to Sub-mm3 Autonomous Systems," in Nanotech 2008 Proceedings, June 2008.
21. V.S. Vasilyev, J.R. Reid, and R.T. Webster, "Microfabrication of Si/SiO_2–Spherical Shells as a Path to Sub-mm^3 Autonomous Robotic Systems," in MRS Fall Meeting, December 2008.
22. J.R. Reid, V.S. Vasilyev, and R.T. Webster, "Three Dimensional Micromachining for Millimeter-wave Circuits," in WAMICON 2009, April 2009.

Patents

1. Patent # 7,002,673, *Optical strain gage compatible with fiber optic systems*, Everett E. Crisman, 27 August 2004.
2. Patent # 7,283,347, *Low cost digital variable capacitor,* J Robert Reid, 16 October 2007.
3. Patent # 7,485,908, *Insulated Gate Silicon Nanowire Transistor and Method of Manufacture*, A. F. M. Anwar and Richard T. Webster, 03 February 2009.

Presentations

1. J. R. Reid "Simulation and measurement of dielectric charging in electrostatically actuated capacitive microwave switches," *Modeling and Simulation of Microsystems (MSM)* p 250, 2002.
2. A. F. M. Anwar, R. T. Webster, S. Wu, S. S. Islam and A. Ahmed, "III-V High Frequency HEMTs," (Invited Lecture) XI th International Workshop on the Physics of Semiconductor Devices, Delhi, India, December 2001.
3. A. F. M. Anwar, R. T. Webster, S. Wu, S. S. Islam and A. Ahmed "GaN and InP Based HEMTs," (Invited Lecture) Electrical and Electronic Engineering Department, BUET, Dhaka, Bangladesh, December 24, 2001.
4. B. Crossley, "Millimeter Wave Imaging and Detection Technology," 2002 IEEE Conference on Technologies for Homeland Security, April 23, 2002.
5. J.R. Reid, "Dielectric Charging Effects on Capacitive MEMS Actuators", Invited presentation at IEEE MTT, Special session on modeling and simulation of RF MEMS switches, Seattle, WA, June 2002.
6. E. E. Crisman, J. S. Derov, O. J. Gregory, and W. B. Euler, "Optical Wave Guide Sensor for Structure Health & Damage Assessment," The Twentieth Transducer Workshop, Wright Patterson Air Force Base, Dayton, OH, June 2002.
8. J.R. Reid, "RF MEMS for Antenna Applications", Short Course at the IEEE APS Annual meeting, San Antonio, TX, July 2002.
9. B. Crossley, "Electromagnetic Technology Seminar on Millimeter Wave Sensor Technologies," AFRL/SNHA Seminar Series #74. July 9, 2002.
10. J.R. Reid, "Simulation and Measurement of Dielectric Charging in Electrostatically Actuated Capacitive Microwave Switches", Invited presentation at the Annual AFRL MEMS Meeting, Hanscom AFB, MA, August, 2002.
11. R. T. Webster, A. F. M. Anwar, J. L. Heaton, K. Nichols, and S. Duncan, "AlGaAsSb/InGaAsSb/AlGaAsSb Metamorphic HEMTs," 2002 Lester Eastman Conference on High Performance Devices, Newark, DE, August 2002.
12. J.R. Reid, "Air Force Interests in RF MEMS Switches," presented at DOD workshop on RF MEMS Switches, Dulles, VA, 13 Jan 2003.

13. E. E. Crisman, J. Derov, A. Drehman and B. Crossley, "Large Pyroelectric Response From Reactively Sputtered Of Aluminum Nitride Thin Films" presented to University of Rhode Island Faculty Research Series, 11 Sep 2003.
14. E. E. Crisman, J. S. Derov, G. Barchard, O. J. Gregory and W. Euler, "Optical Strain Sensor Adjustable for Ranges To 5000 μ-Strain," presented to University of Rhode Island Faculty Research Series, 11 Sep 2003.
15. R.A. Coutu Jr., L.A. Starman, J.R. Reid, and P.E. Kladitis, "Finite Element Modeling and Simulation of Micro-Switch Pull-in Voltage and Contact Force," in *Eurosensors*, Sept. 2003.
16. L. A. Starman, "RF MEMS Switches for Antenna Applications," Worcester Polytechnic Institute, at Mechanical Engineering Department Seminar, 26 March 2004.
17. J. R. Reid, "Microwave MEMS Research at the Air Force Research Laboratory: Metal Contact MEM Switches," at University of Connecticut Engineering Seminar, 20 Jun 2004.
18. L. R. P. Porisch, L. A. Starman, and J. R. Reid, "Experimental and computational characterization of deflection and residual stress in multilayer Nickel microcantilevers," 15th International Invitational Symposium on the Unification of Analytical, Computational, and Experimental Solution Methodologies (UACEM): UACEM in MEMS and Nanotechnology, Springfield MA, October 27-29, 2004.
19. J.R. Reid, "Micromachining 3D Structures for Micro-Robots", Invited presentation at Carnegie Mellon University, Aug 2005.

LIST OF SYMBOLS, ABBREVIATIONS, AND ACRONYMS

2DEG	two dimensional electron gas
3D	Three Dimensional
Å	angstrom
α_n	impact ionization coefficient
C	Centigrade
cm	centimeter
CMOS	complementary metal oxide semiconductor
C-V	Capacitance-Voltage
dB	decibel
DC	Direct Current
dT/dt	time derivative of temperature
EPR	electron paramagnetic resonance
eV	electron volt
f_F	femtofarad
f_{MAX}	maximum oscillation frequency
f_T	current gain cutoff frequency
FTIR	Fourier Transform Infrared Spectroscopy
g_D	transconductance
GHz	gigahertz
HEMT	High Electron Mobility Transistor
Hz	hertz
ID	drain current
I_{HOLE}	hole current
III-V	compound from columns three and five of the periodic table
IR	infrared
K	Kelvin

kG	kilogauss
kV	kilovolt
L	Length of high field region
M	meter
MEMS	Micro Electro Mechanical
MESFET	Metal Semiconductor Field Effect Transistor
MHEMT	Metamorphic High Electron Mobility Transistor
mm	millimeter
MMIC	monolithic microwave integrated circuit
mW	milliwatt
MΩ	megaohm
PVDF	poly vinylidene fluoride
RF	Radio Frequency
rms	root mean square
s	second
SEM/EDS	scanning electron microscope/electron diffraction spectroscopy
SOI	silicon on oxide
SPDT	single pole double throw
SPST	single pole single throw
UV	ultraviolet
V	Volts
V_D	drain voltage
$V_{D,sat}$	saturated drain voltage
V_{DC}	Voltage for direct current
V_G	gate voltage
V_{GD}	gate to drain voltage
Ω	ohm
μ	permeability
μm	micrometer